Attosecond time delay in valence photoionization and photorecombination of argon: A time-dependent local-density-approximation study

Maia Magrakvelidze, Mohamed El-Amine Madjet, Gopal Dixit, Misha Ivanov, and Himadri S. Chakraborty

Phys. Rev. A **91**, 063415 — Published 22 June 2015

DOI: 10.1103/PhysRevA.91.063415

Attosecond time delay in valence photoionization and photorecombination of argon: a TDLDA study

Maia Magrakvelidze,[1] Mohamed El-Amine Madjet,[2] Gopal Dixit,[3] Misha Ivanov,[3,4] and Himadri S. Chakraborty[1,*]

[1] *Department of Natural Sciences, D.L. Hubbard Center for Innovation and Entrepreneurship, Northwest Missouri State University, Maryville, Missouri 64468, USA*
[2] *Qatar Environment and Energy Research Institute, Qatar Foundation, P.O Box 5825, Doha, Qatar*
[3] *Max Born Institute, Max-Born-Strasse 2A, 12489 Berlin, Germany*
[4] *Blackett Laboratory, Imperial College London, London SW7 2AZ, United Kingdom*

(Dated: May 4, 2015)

We determine and analyze the quantum phases and time delays in photoionization and photorecombination of valence $3p$ and $3s$ electrons of argon using the Kohn-Sham local density functional approach. The time-dependent local density approximation (TDLDA) is used to account for the electron correlation. Resulting attosecond Wigner-Smith time delays show excellent agreements with two recent independent experiments on argon that measured the relative $3s-3p$ time delay in photoionization [Physical Review Letters **106**, 143002 (2011)] and the delay in $3p$ photorecombination [Physical Review Letters **112**, 153002 (2014)].

PACS numbers: 32.80.Fb, 61.48.-c, 31.15.E-

I. INTRODUCTION

Technological advances in producing the isolated attosecond pulse [1, 2] and attosecond pulse trains [3, 4] have facilitated pump-probe experiments to resolve the photoionization (PI) process in real time [5–9]. In attosecond streaking measurements, following the ionization by an extreme ultraviolet (XUV) pump pulse, photoelectrons are boosted by the infrared (IR)-probe vector potential to different final momenta as a function of pump-probe time delay, which are then mapped into a spectrogram. Theoretical modeling of such spectrograms extracts the time delay associated with PI. For instance, the relative time delay between photoelectrons emitted from $2s$ and $2p$ orbitals of atomic neon [5] as well as between photoelectrons from conduction and valence bands in bulk metals have been measured using streaking methods [8, 9]. Introducing a coincidence technique of photoelectron detection, multiple streaking traces can be determined in a single experiment for emissions from various atomic orbitals or from different gas species in a mixed sample [10]. In the interferometric measurements, namely RABITT (reconstruction of attosecond beating by interference of two-photon transitions) [3], photoelectrons emitted by odd harmonics of an XUV pulse train subsequently absorb or emit an IR photon. This produces even harmonic sidebands in the spectrogram. The ionization time delay is then obtained by the ratio of the difference of the measured phases at consecutive sidebands and the harmonic separation. Important recent measurements using RABITT technique include relative delay between argon $3s$ and $3p$ photoemission [6, 7] as well as between emissions from various noble gas atoms [11].

The additional delay introduced by the IR probe pulse via the so called continuum-continuum coupling or Coulomb-laser coupling can be calculated separately and subtracted from the measured result, yielding the Wigner-Smith delay associated with PI [12–14]. This is because, the phase-frequency difference approach mentioned above approximates the energy differential of the phase of the PI amplitude which defines the Wigner-Smith delay [15, 16]. This delay is the excess time, positive or negative, spent by the electron to reach the continuum in addition to the time it would take in the absence of interactions between the continuum electron and the target. Therefore, attosecond time delay is an important probe of dynamical correlation effects in PI processes. Several theoretical methods employed to explain experimental $3s-3p$ relative delay in argon were only partially successful to reproduce measurements [6, 7, 17–20], with the exception of multi-configurational Hartree-Fock that had a better success [21].

Recently, the phase and the group delay associated with photorecombination (PR) of argon $3p$ electron at energies that include the $3p$ Cooper minimum have been measured using the combination of high-harmonic generation (HHG) and RABITT methods [22]. Observations of the Cooper minima in HHG spectra of various atoms and molecules have been a subject of recent work [23–28]. The presence of such minima in HHG spectra indicates that the structure of the sample can be probed despite the presence of a strong IR pulse during recombination. The assumption of time-reversal symmetry between PR and PI forms the basis of the principle of detailed balance [29]. This leads to a one-to-one correspondence between PR and PI [30, 31] which permits the retrieval of structural and dynamical information of the sample from HHG spectra.

The purpose of the present paper is to provide a detailed theoretical analysis of the phase and Wigner-Smith time delay associated with PI and PR processes. We report the calculation of these phases and delays for argon

* himadri@nwmissouri.edu

using the time-dependent local density approximation (TDLDA) method, and show that the results successfully describe recent PI [6, 7] and PR [22] measurements. The argon atom is one of the most studied system for HHG and attosecond pulse generation, and has a $3s$ and a $3p$ Cooper minimum at, respectively, 42 eV and 48 eV photon energy in the PI cross section [32, 33] (the latter yields a 53±3-eV minimum in the HHG spectra [23–25]). Our study spotlights the importance of the second dipole-allowed channel at energies near the Cooper minimum of a given channel with same initial orbital and, in general, stresses the adequacy of TDLDA method to interpret RABITT measurements. Results also add reliability to recent TDLDA predictions [19, 34, 35] of the PI time delay in fullerene materials.

This paper is structured as follows. Section II includes three subsections: A) the description of PI and PR within the independent particle model – the local density approximation (LDA); B) the essentials of TDLDA, which incorporates important electron-electron correlations; and C) an alternative discussion about the electron correlation in PI and PR via the interchannel coupling formalism by Fano. Section III discusses numerical results and their comparisons with recent measurements. Conclusions are presented in Sec. IV.

II. THEORETICAL PERSPECTIVES

A. Independent particle model

Choosing the photon polarization along z-axis, the PI and PR dipole transition amplitudes in a single channel approximation, which omits electron correlations, are:

$$d_{\rm PI} = \langle \psi^-_{kl'} | z | \phi_{nl} \rangle, \tag{1a}$$

and

$$d_{\rm PR} = \langle \phi_{nl} | z | \psi^+_{kl'} \rangle. \tag{1b}$$

Here, k is the momentum of the continuum electron and z is the one-body dipole operator. ϕ_{nl} is the bound wavefunction of the target and $\psi_{kl'}$ with $+(-)$ represents outgoing (incoming) spherical continuum wavefunction as

$$\psi^\pm_{kl'}(\mathbf{r}) = (8\pi)^{\frac{3}{2}} \sum_m e^{\pm i\eta_{l'}} R_{kl'}(r) Y_{l'm}(\mathbf{\Omega_r}) Y^*_{l'm}(\mathbf{\Omega_k}) \tag{2}$$

with $l' = l \pm 1$. In Eq. (2), the scattering phase $\eta_{l'}(k)$ contains contributions from both short-range and Coulomb potentials, and $R_{kl'}$ is the radial continuum wave. Since $(\psi^+)^* = \psi^-$, it follows from Eqs. (1) that $d_{\rm PI} = d_{\rm PR}$, satisfying the time-reversal symmetry between PI and PR.

We calculate amplitudes d [Eqs. (1)] using the independent particle LDA method [36–38]. Here the LDA potential, using the single-particle density $\rho(\mathbf{r})$,

$$V_{\rm LDA}(\mathbf{r}) = -\frac{z}{r} + \int d\mathbf{r}' \frac{\rho(\mathbf{r}')}{|\mathbf{r}-\mathbf{r}'|} + V_{\rm XC}[\rho(\mathbf{r})] \tag{3}$$

uses Leeuwen-Baerends (LB) exchange-correlation functional ($V_{\rm XC}$) [39], which provides accurate asymptotic description of the ground state potential. LDA self-consistently includes an average interaction with the ionic core, and obtains the ground and continuum single-electron states for various angular momenta in a mean-field approximation. Thus, LDA is akin to the Hartree-Fock method, albeit an approximation to the (non-local) exchange in a local frame.

We note the following in our LDA results. The absolute value of the amplitude, $|d|$, of PI and PR dipole channels, $3p \leftrightarrow kd$, show minima at an energy of about 37 eV, below the energy of the regular $3p$ Cooper minimum. In Fig. 2(a), such a minimum in $3p \to kd$ LDA cross section is seen, but no minimum is found in $3s \to kp$. Eqs. (1) include LDA radial matrix elements, $\langle R_{kd,ks}|z|R_{3p}\rangle$ and $\langle R_{3p}|z|R_{kd,ks}\rangle$, respectively, for PI and PR. The scattering phase [η in Eq. (2)] of PI and PR does not have any structure at these energies. As the radial matrix element associated with $3p \to kd$ transition changes its sign, the total phase corresponding to the total matrix element has a sharp and discontinuous phase-jump at the Cooper minimum, which is at a lower energy compared to the experimentally observed minimum. Note that only scattering phase is considered at the mean-field approximation and our LDA results (not shown) are consistent with the Hartree-Fock results for argon PI [18, 40]. We show below that when the electron correlation is included via the complex induced potential in TDDLA [see Eq. (4)], the position of the Cooper minimum in the cross-section and the variation of the total phase of the radial matrix element at the Cooper minimum reproduce the measured results.

B. Time-dependent local density approximation

The time-dependent local density approximation (TDLDA), used here to calculate the full transition amplitude, includes many-electron effects and utilizes the advanced, G^+ (for PI), and retarded, G^- (for PR), Green's functions [37, 41, 42]. In a linear response frame, as TDLDA, the PI and PR amplitudes formally read as

$$D_{\rm PI} = \langle \psi^-_{kl'} | \delta V^*_+ + z | \phi_{nl} \rangle = d_{\rm PI} + \langle \delta V^*_+ \rangle, \tag{4a}$$

and

$$D_{\rm PR} = \langle \phi_{nl} | z + \delta V_- | \psi^+_{kl'} \rangle = d_{\rm PR} + \langle \delta V_- \rangle. \tag{4b}$$

Here, $\delta V_\pm$ are complex induced potentials which account for electron correlations. In TDLDA, $(z + \delta V_\pm)$ are proportional to the induced frequency-dependent changes in the electron density [43]. This change is

$$\delta\rho_\pm(\mathbf{r}';\omega) = \int \chi_\pm(\mathbf{r},\mathbf{r}';\omega) z d\mathbf{r}, \tag{5}$$

where the full susceptibility χ builds the dynamical correlation from the independent particle LDA susceptibilities

$$\chi^0_\pm(\mathbf{r},\mathbf{r}';\omega) = \sum_{nl}^{occ} \phi^*_{nl}(\mathbf{r})\phi_{nl}(\mathbf{r}')\; G^{(\pm)}(\mathbf{r},\mathbf{r}';\epsilon_{nl}+\omega) + \sum_{nl}^{occ} \phi_{nl}(\mathbf{r})\phi^*_{nl}(\mathbf{r}')\; G^{(\pm)*}(\mathbf{r},\mathbf{r}';\epsilon_{nl}-\omega) \quad (6)$$

via the matrix equation $\chi = \chi^0[1-(\partial V/\partial\rho)\chi^0]^{-1}$ involving the variation of the ground-state potential V with respect to the ground-state density ρ. The radial components of the full Green's functions in Eq. (6) are constructed with the regular (f_L)and irregular (g_L) solutions of the homogeneous radial equation

$$\left(\frac{1}{r^2}\frac{\partial}{\partial r}r^2\frac{\partial}{\partial r} - \frac{L(L+1)}{r^2} - V_{\rm LDA} + E\right) f_L(g_L)(r;E) = 0 \quad (7)$$

as

$$G^{\pm}_L(r,r';E) = \frac{2 f_L(r_<;E)h^{(\pm)}_L(r_>;E)}{\text{Wronskian}[f_L,h_L]} \quad (8)$$

where $h^{(\pm)}_L = g_L \pm i\, f_L$ are complex conjugate combinations. Obviously, the latter fact, along with Eqs. (5-8), demonstrates that $\delta V^*_+ = \delta V_-$, thus confirming $D_{\rm PI} = D_{\rm PR}$. Note that TDLDA thus includes the dynamical correlation by improving upon the mean-field LDA basis.The numerical results presented in this paper are obtained using TDLDA method only.

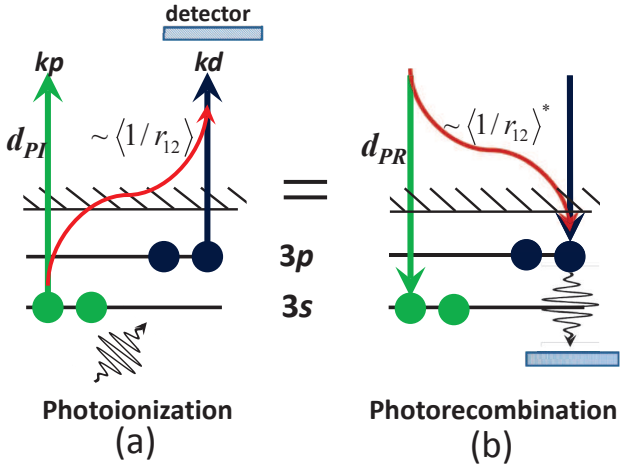

FIG. 1. (Color online). Schematics of total photoamplitudes for transitions of the $3p$ electron. Vertical arrows are single channel matrix elements for $3p$ and $3s$ [Eqs. (1)], while curved arrows represent the coupling via the interchannel matrix elements $\langle 1/r_{12}\rangle$ [see text after Eq. (10)]. The detector on each panel identifies the channel being observed in this two-channel interaction model.

C. Electron correlations via interchannel coupling

Before discussing our numerical results, we present Fano formalism of interchannel coupling, which is used to interpret the results.

For photon energies of current interest, the dominant correlation emerges between valence $3p$ and $3s$ channels, since argon inner electrons are too deeply bound. An elegant way to interpret the dynamical correlation is through the coupling between independent particle channels as described by Fano [44]. For instance, in the first order perturbation theory, to approximate the "exact" continuum wavefunction of the $3p \to kd$ channel, coupled to the degenerate $3s \to kp$ (perturbing) channel, we obtain for the corrected wavefunction:

$$|\Psi^-_{kd}(E)\rangle = |\psi^-_{kd}\rangle + \lim_{\lambda\to 0}\int dE' \frac{\langle\tilde\psi^-_{kd}|\frac{1}{r_{12}}|\tilde\psi^-_{k'p}\rangle}{E-E'+i\lambda}|\psi^-_{k'p}\rangle \approx |\psi^-_{kd}\rangle + c\langle\tilde\psi^-_{kd}|\frac{1}{r_{12}}|\tilde\psi^-_{k'p}\rangle|\psi^-_{kp}\rangle. \quad (9)$$

Here, $\tilde\psi$ are two-electron wavefunctions that include both bound and continuum states of an independent particle channel, and c is a complex number which includes the contributions of pole and principal value terms, both accumulated near $E' = E$. In the second step above, we approximate the energy integral by the leading contribution at $E' = E = k^2/2$ for simplicity. Using Eq. (9) in the form (1a), the correlation-corrected PI amplitude can be written as

$$D_{3p\to kd} = \langle\Psi^-_{kd}|z|\phi_{3p}\rangle = d_{3p\to kd} + c\langle\tilde\psi^-_{kp}|\frac{1}{r_{12}}|\tilde\psi^-_{kd}\rangle d_{3s\to kp}, \quad (10)$$

in which the complex *interchannel coupling matrix element*, $\langle 1/r_{12}\rangle$, with a two-body operator embodies the fraction of the independent particle $3s \to kp$ strength that transfers, via correlation, to the observed $3p \to kd$ channel. Note, since both bound as well as continuum wavefunctions constitute $\tilde\psi$, this correlation incorporates the continuum-continuum interaction between the "detected" d and "perturbing" p photoelectrons augmented by the strong $3p$-$3s$ bound state overlap. In specific, the correlation is expected to dominate the Cooper-minimum region where the strength of the observing channel is small. Fig. 1(a) is a phenomenological representation of Eq. (10) for the detection of $3p$ electrons where the vertical arrows denote independent particle PIs and the curved arrow is $3s$-to-$3p$ correlation contribution.

The corresponding *time-reversed* photoamplitude with interchannel coupling, plugging the outgoing version of Eq. (9) in the form (1b), can likewise be found as

$$D_{3p\leftarrow kd} = \langle\phi_{3p}|z|\Psi^+_{kd}\rangle = d_{3p\leftarrow kd} + c^*\langle\tilde\psi^+_{kd}|\frac{1}{r_{12}}|\tilde\psi^+_{kp}\rangle d_{3s\leftarrow kp}, \quad (11)$$

which is sketched in Fig. 1(b) and can be shown to exactly equal to its time-forward counterpart, Eq. (10), since $(\psi^+)^* = \psi^-$ and $d_{\rm PI} = d_{\rm PR}$. Obviously, Eq. (11) or

Fig. 1(b) is the $3p \leftarrow kd$ PR process correlation-modified by its coupling with $3s \leftarrow kp$. One can likewise show the equality of PI versus PR amplitudes by choosing to observe the $3s$ channel that couples to a $3p$ channel.

Note that the correlation expressed in the wavefunction via the interchannel coupling in Eq. (9) effectively reincarnates in the operator δV in Eqs. (4). In fact, $\langle \delta V \rangle$ corresponds to the correlation contribution in Eq. (10) [45].

III. RESULTS, DISCUSSIONS AND COMPARISONS WITH MEASUREMENTS

The total, $3p$, and $3s$ PI cross sections for argon, obtained within TDLDA, are in very good agreement with the measurements [32, 33] as shown previously by us [19]. The PR cross sections are derivable directly from PI results by incorporating the principle of detailed balance. The TDLDA phase (Γ) of the amplitude D is the sum of the LDA phase ($l'\frac{\pi}{2} + \eta$) [Eq. (2)] and the phase (the correlation phase) of the complex radial matrix element embedded in D. These phases for channels involving $3p$ and $3s$ electrons are shown in Fig. 2(b). At energies directly above the ionization thresholds, η is dominated by the Coulomb phase. The phases of $3s \rightarrow kp$ and $3p \rightarrow kd$ exhibit rapid variations at their respective Cooper minima at 42 and 48 eV. These minima are also seen in the TDLDA cross sections for PI in Fig. 2(a). Evidently, the correlation blue-shifts the $3p$ Cooper minimum from its LDA position (37 eV). The correlation now also introduces a phase variation at the zero of Re(D), since D is now complex due to the complex δV in Eq. (4a). In the Fano formalism, the non-trivial origin of this complex D is the interchannel coupling matrix element in Eq. (10).

Further, for the $3s$ ionization, one rewrites Eq. (10) for $3s \rightarrow kp$ modified by the coupling with $3p \rightarrow kd$; this entails d's on r.h.s. to interchange and the interchannel coupling matrix element to conjugate. Two important consequences emerge: (i) The coupling term now directly inserts a minimum in TDLDA $3s$ channel (Fig. 2(b)) via the LDA amplitude (d) of $3p \rightarrow kd$ that has a minimum and is stronger enough than the $3s$ channel to dramatically modify it through the interchannel coupling; (ii) The complex conjugation of interchannel coupling matrix element explains why there are opposite variations in $3p$ and $3s$ phases at their respective minima in Fig. 2(b). Similar relative trend is also found by random-phase approximation with exchange [18]. The upshift (positive delay, as will be shown below) of $3s$ phase points a slower emergence of the $3s$ electron, while the downshift of $3p$ suggests the opposite.

Until recently, there was an ambiguity about the direction of relative variations between $3p$ and $3s$ phases at their Cooper minima. Schoun *et al.* have measured the variation of argon $3p$ phase for the PR process across the Cooper minima for the first time [22]. The correlation phase in the previous calculation was not correct [19]. In the present calculation, this error has been rectified by using the correct sign of the imaginary part of the overall term. Note further in Fig. 2(b) that the $3p \rightarrow ks$ phase is large and rather monotonic as a function of energy, since no Cooper minimum exists in this channel. A crucial consequence of this fact will be recognized in the following.

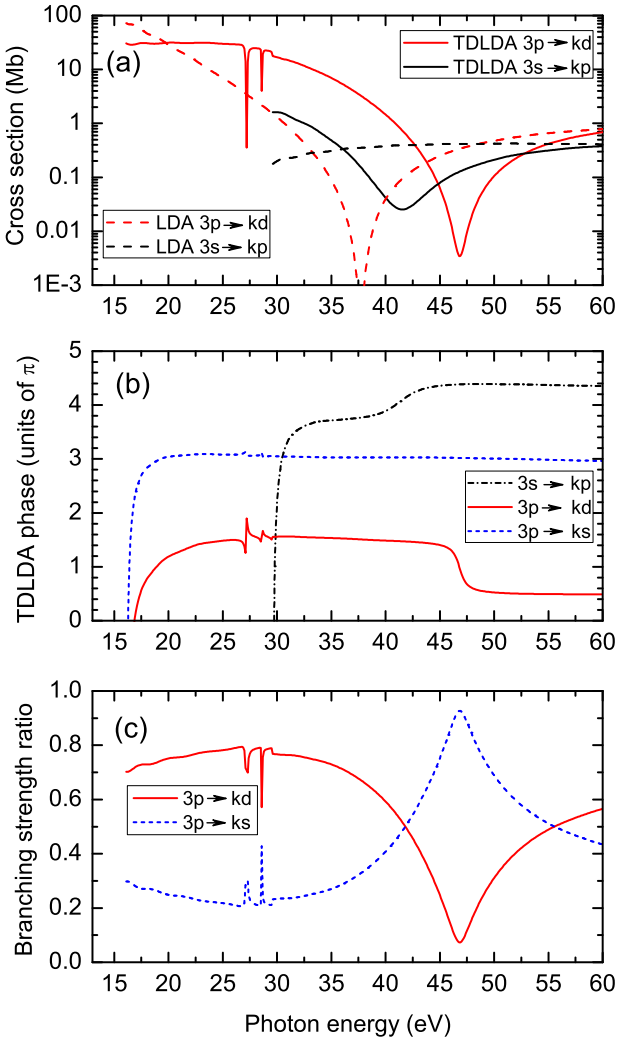

FIG. 2. (Color online). (a) LDA and TDLDA cross sections for $3p \rightarrow kd$ and $3s \rightarrow kp$ photoionization channels. (b) TDLDA phases for $3p \rightarrow kd, ks$ channels. Structures between 25 to 30 eV in $3p$ curves are from $3s$ excitations Rydberg resonances. (c) Branching strength ratios (see Eq. (14)) are used in weighted-averaging the phases of two dipole channels of $3p$ electrons.

In streaking experiments, one measures the delay associated with the angle-resolved phase of the *full* $3p$ amplitude of emissions at a solid angle Ω_k [46]. Ignoring the

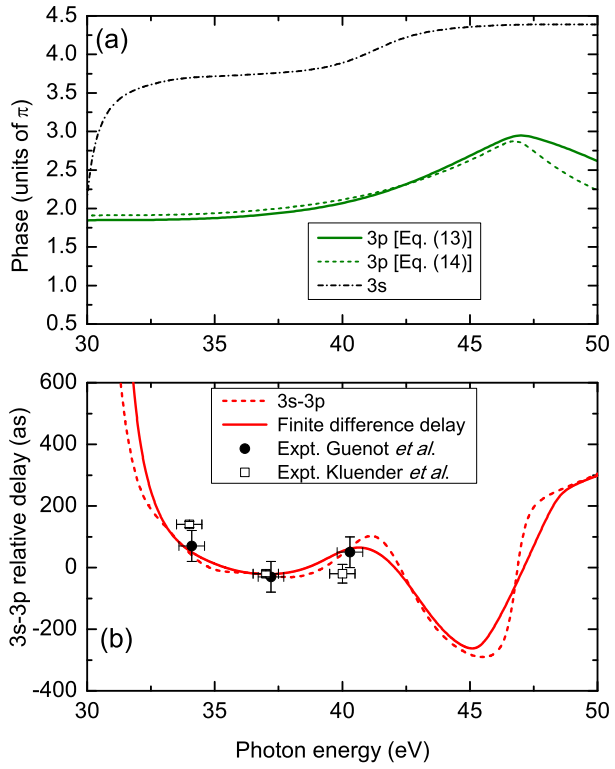

FIG. 3. (Color online). (a) TDLDA 3s phase and total 3p phase calculated using Eq. (13) (solid green line) and Eq. (14) (dotted green line). (b) TDLDA relative 3s−3p Wigner-Smith and "finite difference" time delays, and their comparison with the measured relative delays by RABITT method (solid circles, Ref. [7]; open squares, Ref. [6]).

phase of the spherical harmonics, this can be written as,

$$\Gamma_{3p}(\Omega_k) = \arg[|D_{3p\to kd}(\Omega_k)|\exp(i\Gamma_{3p\to kd}) + |D_{3p\to ks}(\Omega_k)|\exp(i\Gamma_{3p\to ks})]. \quad (12)$$

In a non-angle-resolved measurement such as RABITT, the total amplitude is close to the direct sum of the dipole matrix elements $|D|$'s over Ω_k in the above equation. Since for a given channel $\int d\Omega_k |D_{3p\to kd(s)}(\Omega_k)|^2 \sim \sigma_{3p\to kd(s)}$, we approximate the integrals overs $|D|$'s by the square root of respective channel cross sections. The TDLDA 3p phase is thus calculated by

$$\Gamma_{3p} = \arg[\sqrt{\sigma_{3p\to kd}}\exp(i\Gamma_{3p\to kd}) + \sqrt{\sigma_{3p\to ks}}\exp(i\Gamma_{3p\to ks})]. \quad (13)$$

In effect, instead of summing the angle-dependent moduli of each channel amplitude, the square root of the sum of their squares is used. Even though the scheme thus neglects the cross terms (interference) among emissions in different directions (by choosing only the self terms), we show that the results explain the measured data obtained in RABITT techniques very well.

Now, we model Eq. (13) in an approximate form to develop some insights as:

$$\Gamma_{3p} \approx \frac{\sqrt{\sigma_{3p\to kd}}}{S}\Gamma_{3p\to kd} + \frac{\sqrt{\sigma_{3p\to ks}}}{S}\Gamma_{3p\to ks}, \quad (14)$$

where $S = \sqrt{\sigma_{3p\to kd}} + \sqrt{\sigma_{3p\to kd}}$. Although, in general, Eq. (14) may have a limited range of validity, but as demonstrated in Fig. 3a, Eqs. (13) and (14) agree numerically within about a 90% accuracy for σ's and Γ's over the current energy range. The advantage of the form (14) is that it explicitly shows the energy-dependent fractions, the branching strengths, of channel-phases in Γ_{3p}. Figure 2(c) presents these branching strengths in Eq. (14) which show the influence of the 3p Cooper minimum. Note that the branching strengths should be identical for PI and PR, since the coefficients from detailed balance cancel out in the ratio. The total 3p phase, thus averaged, is presented in Fig. 3(a) which shows an energy gradient similar to that of the 3s phase in the range from above the 3s Coulomb region near its threshold up to the 3p Cooper minimum. Why does this happen in spite of the opposite variations in 3p and 3s phases near their minima in Fig. 2(b)? This is because while the $3p \to kd$ channel is generally strong, it gets very weak near its Cooper minimum so the $3p \to ks$ phase, having a characteristic higher value, dominates (see Eq. (14)). Indeed, as evident in Fig. 2(c), while the $3p \to kd$ channel dominates below 40 eV of photon energy, both channels become comparable around 42 eV. With higher energy, this trend continues and enables $3p \to ks$ to eventually contribute about 90% of the total strength right at the Cooper minimum. Past the minimum, however, the $3p \to kd$ channel recovers and regains its dominance above 55 eV. This reversal of relative strengths at the minimum has an important consequence which we point out below. The following results use Eq. (13) for the 3p phase.

The energy-derivative of 3s and 3p phases, their Wigner-Smith time delays, is performed to calculate the relative time delay between 3s and 3p photo electrons. Figure 3(b) presents the calculated relative delay in TDLDA and its comparison with the measurements [6, 7]. TDLDA and the measured delays are in very good agreements, remarkably even at the highest energy, closest to the 3s Cooper minimum, in the experiment. In fact the TDLDA result describes the most recent measurements [7] almost perfectly. Small relative delays at all three measured energies are the consequence of similar energy-gradients of the 3s and the total 3p phases in Fig. 3(a). The RABITT measurement used IR probe pulse of 1.55-eV (800-nm) energy to extract the time delay from measured phases (Γ) in a finite difference approach: $\tau(E) = [\Gamma(E+\omega) - \Gamma(E-\omega)]/2\omega$. In order to mimic this experimental procedure, we also apply finite-differencing of our TDLDA phases (Fig. 3(a)) using 1.55-eV half-steps. Resulting "finite difference" delay is presented in Fig. 3(b) that retains the quality of agreement with the data points. It is further seen that the TDLDA predicts structures from the 3p Cooper mini-

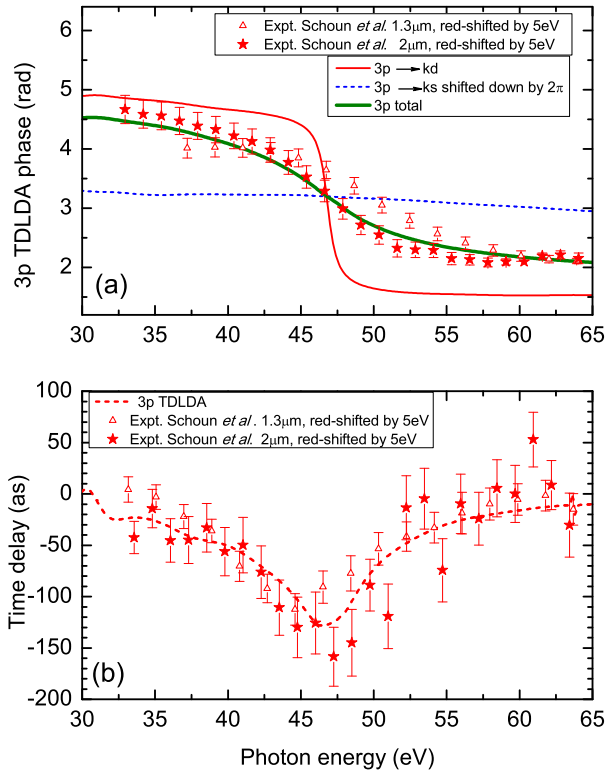

FIG. 4. (Color online). (a) Total $3p$ TDLDA phase, an admixture of $3p \to kd, ks$ phases using Eq. (14) with $3p \to ks$ shifted down by 2π, is compared with measured phases for $3p$ photorecombination [22], but shifted upward by 4 rad. (b) The same as in (a) but for $3p$ Wigner-Smith time delay. Experimental results are red-shifted by 5 eV in both the cases (open triangles, 1.3 μm; stars, 2 μm).

mum at higher energies which can be accessed by the attosecond interferometric metrology.

In the following, we compare our TDLDA phase for the two $3p$ channels with the recently measured absolute $3p$ phase and associated time delay across the $3p$ Cooper minimum in the PR process [22]. Figure 4(a) shows that $3p \to kd$ TDLDA phase qualitatively matches with the measured phase, albeit a sharper energy-variation for TDLDA while the measurement shows a softer behavior. We adopt the similar scheme as used in [22] to soften the total $3p$ phase using the s-wave phase. This required the folding of $3p \to ks$ phase onto the range of $0 - 2\pi$ rad (Fig. 4(a)) before applying Eq. (13). The result provided a softer variation of the total $3p$ phase around the minimum which then falls in a very good agreement with the measurement [22], as seen in Fig. 4(a). Note that the experimental phase was red-shifted by 5 eV. It was also needed to shift the measured data up by 4 radian for comparison. This is because since the actual observable measured is the derivative of the phase, there is an arbitrary constant shift of the total phase. Respective Wigner-Smith delays for $3p$ PR, TDLDA versus experiment, are then compared in Fig. 4(b) that also exhibits nice agreements. We have further calculated the finite difference TDLDA delays with 1.3-μm and 2.0-μm half-steps, which are experimental IR photon energies [22], but obtained virtually the same results.

IV. CONCLUSIONS

To summarize, a detailed theoretical study of argon valence photoionization and photorecombination spectral phases and associated Wigner-Smith time delays has been carried out within the TDLDA methodology. A notion of interchannel coupling based on Fano formalism to account for electron correlations is introduced to aid the interpretation of the result and to support the generally accepted consensus that PI is a time-reversal process of PR. Numerical results for the phases reveal structures at respective $3p$ and $3s$ Cooper minima with opposite energy variations, resulting from the correlation based on mutual couplings between $3p$ and $3s$ channels. The relative $3s - 3p$ Wigner-Smith time delay is computed and found in excellent agreement with recent RABITT measurements. TDLDA absolute phase and delay results for $3p$ transition are also found in very good accord with measured data using HHG+RABITT where, however, the s-wave phase was required to be folded – a fact that needs further investigation. As a final remark, TDLDA calculations using explicit corrections for electron self-interactions [43] with a different exchange-correlation functional [47] produced qualitatively similar results to those presented here.

ACKNOWLEDGMENTS

The research is supported by the NSF, USA.

[1] M. Hentschel, R. Kienberger, C. Spielmann, G. A. Reider, N. Milosevic, T. Brabec, P. Corkum, U. Heinzmann, M. Drescher, and F. Krausz, Nature **414**, 509 (2001).
[2] E. Goulielmakis, M. Schultze, M. Hofstetter, V. S. Yakovlev, J. Gagnon, M. Uiberacker, A. L. Aquila, E. M. Gullikson, D. T. Attwood, R. Kienberger, F. Krausz, and U. Kleineberg, Science **320**, 1614 (2008).
[3] P. M. Paul, E. S. Toma, P. Breger, G. Mullot, F. Augé, P. Balcou, H. G. Muller, and P. Agostini, Science **292**, 1689 (2001).
[4] Y. Mairesse, A. De Bohan, L. J. Frasinski, H. Merdji, L. C. Dinu, P. Monchicourt, P. Breger, M. Kovačev,

R. Taïeb, B. Carré, H. G. Muller, P. Agostini, and P. Salires, Science **302**, 1540 (2003).
[5] M. Schultze, M. Fie, N. Karpowicz, J. Gagnon, M. Korbman, M. Hofstetter, S. Neppl, A. L. Cavalieri, Y. Komninos, T. Mercouris, C. A. Nicolaides, R. Pazourek, S. Nagele, J. Feist, J. Burgdrfer, A. M. Azzeer, R. Ernstorfer, R. Kienberger, U. Kleineberg, E. Goulielmakis, F. Krausz, and V. S. Yakovlev, Science **328**, 1658 (2010).
[6] K. Klünder, J. M. Dahlström, M. Gisselbrecht, T. Fordell, M. Swoboda, D. Guénot, P. Johnsson, J. Caillat, J. Mauritsson, A. Maquet, R. Taïeb, and A. L'Huillier, Physical Review Letters **106**, 143002 (2011).
[7] D. Guénot, K. Klünder, C. L. Arnold, D. Kroon, J. M. Dahlström, M. Miranda, T. Fordell, M. Gisselbrecht, P. Johnsson, J. Mauritsson, E. Lindroth, A. Maquet, R. Taïeb, A. L'Huillier, and A. S. Kheifets, Physical Review A **85**, 053424 (2012).
[8] S. Neppl, R. Ernstorfer, E. M. Bothschafter, A. L. Cavalieri, D. Menzel, J. V. Barth, F. Krausz, R. Kienberger, and P. Feulner, Physical Review Letters **109**, 87401 (2012).
[9] A. L. Cavalieri, N. Mller, T. Uphues, V. S. Yakovlev, A. Baltuska, B. Horvath, B. Schmidt, L. Blmel, R. Holzwarth, S. Hendel, M. Drescher, U. Kleineberg, P. M. Echenique, R. Kienberger, F. Krausz, and U. Heinzmann, Nature **449**, 1029 (2007).
[10] M. Sabbar, S. Heuser, R. Boge, M. Lucchini, L. Gallmann, C. Cirelli and U. Keller, http://arxiv.org/abs/1407.6623v1 (2014).
[11] D. Guénot, D. Kroon, E. Balogh, E. W. Larsen, M. Kotur, M. Miranda, T. Fordell, P. Johnsson, J. Mauritsson, M. Gisselbrecht, K. Varju, C. L. Arnold, T. Carette, A. S. Kheifets, E. Lindroth, A. L'Huillier and J. M. Dahlström, Journal of Physics B: Atomic, Molecular and Optical Physics **47**, 245602 (2014).
[12] M. Ivanov and O. Smirnova, Physical Review Letters **107**, 213605 (2011).
[13] S. Nagele, R. Pazourek, J. Feist, and J. Burgdörfer, Physical Review A **85**, 033401 (2012).
[14] J. M. Dahlström, D. Guénot, K. Klünder, M. Gisselbrecht, J. Mauritsson, A. L'Huillier, A. Maquet, and R. Taïeb, Chemical Physics **414**, 53 (2012).
[15] E. P. Wigner, Physical Review **98**, 145 (1955).
[16] F. T. Smith, Physical Review **118**, 349 (1960).
[17] J. M. Dahlström, T. Carette, and E. Lindroth, Physical Review A **86**, 061402 (2012).
[18] A. S. Kheifets, Physical Review A **87**, 063404 (2013).
[19] G. Dixit, H. S. Chakraborty, and M. E. Madjet, Physical Review Letters **111**, 203003 (2013).
[20] J. M Dahlström and E. Lindroth, Journal of Physics B: Atomic, Molecular and Optical Physics **47**, 124012 (2014).
[21] T. Carette, J. M. Dahlström, L. Argenti, and E. Lindroth, Physical Review A **87**, 023420 (2013).
[22] S. B. Schoun, R. Chirla, J. Wheeler, C. Roedig, P. Agostini, L. F. DiMauro, K. J. Schafer, and M. B. Gaarde, Physical Review Letters **112**, 153001 (2014).
[23] H. J. Wörner, H. Niikura, J. B. Bertrand, P. B. Corkum, and D. M. Villeneuve, Physical Review Letters **102**, 103901 (2009).
[24] J. Higuet, H. Ruf, N. Thiré, R. Cireasa, E. Constant, E. Cormier, D. Descamps, E. Mével, S. Petit, B. Pons, Y. Mairesse, and B. Fabre, Physical Review A **83**, 053401 (2011).
[25] J. P. Farrell, L. S. Spector, B. K. McFarland, P. H. Bucksbaum, M. Gühr, M. B. Gaarde, and K. J. Schafer, Physical Review A **83**, 023420 (2011).
[26] A. D. Shiner, B. E. Schmidt, C. Trallero-Herrero, P. B. Corkum, J. C. Kieffer, F. Légaré, and D. M. Villeneuve, Journal of Physics B: Atomic, Molecular and Optical Physics **45**, 074010 (2012).
[27] J. B. Bertrand, H. J. Wörner, P. Hockett, D. M. Villeneuve, and P. B. Corkum, Physical Review Letters **109**, 143001 (2012).
[28] M. C. H. Wong, A. T. Le, A. F. Alharbi, A. E. Boguslavskiy, R. R. Lucchese, J. P. Brichta, C. D. Lin, and V. R. Bhardwaj, Physical Review Letters **110**, 033006 (2013).
[29] L. D. Landau and E. M. Lifshitz, *Quantum Mechanics. Non-relativistic theory*, Pergamon Press: New York, 1965.
[30] T. Morishita, A.-T. Le, Z. Chen, and C. D. Lin, Physical Review Letters **100**, 013903 (2008).
[31] A.-T. Le, R. R. Lucchese, S. Tonzani, T. Morishita, and C. D. Lin, Physical Review A **80**, 013401 (2009).
[32] B. Möbus, B. Magel, K. H. Schartner, B. Langer, U. Becker, M. Wildberger, and H. Schmoranzer, Physical Review A **47**, 3888 (1993).
[33] J. A. R. Samson and W. C. Stolte, Journal of electron spectroscopy and related phenomena **123**, 265 (2002).
[34] T. Barillot, C. Cauchy, P -A. Hervieux, M. Gisselbrecht, S. E. Canton, P. Johnsson, J. Laksman, E. P. Mansson, J. M. Dahlström, M. Magrakvelidze, G. Dixit, M. E. Madjet, H. S. Chakraborty, E. Suraud, P. M. Dinh, P. Wopperer, K. Hansen, V. Loriot, C. Bordas, S. Sorensen and F. Lépine, Physical Review A **91**, 033413 (2015).
[35] M. Magrakvelidze, D. M. Anstine, G. Dixit, M. E. Madjet, and H. S. Chakraborty, Physical Review A (accepted); http://arxiv.org/abs/1409.2910 (2014).
[36] M. E. Madjet, H. S. Chakraborty, and J. -M. Rost, Journal of Physics B: Atomic, Molecular and Optical Physics **34**, L345 (2001).
[37] A. Zangwill and P. Soven, Physical Review A **21**, 1561 (1980).
[38] M. Stener, G. De Alti, G. Fronzoni and P. Decleva Chem. Phys. **222**, 197 (1997).
[39] R. Van Leeuwen and E. J. Baerends, Physical Review A **49**, 2421 (1994).
[40] D. J. Kennedy and S. T. Manson, Physical Review A **5**, 227 (1972).
[41] W. Ekardt, Physical Review B **31**, 6360 (1985).
[42] T. Nakatsukasa, K. Yabana, Journal of Chemical Physics **114**, 2550 (2001).
[43] M. E. Madjet, H. S. Chakraborty, J .M. Rost, and S .T. Manson, Journal of Physics B: Atomic, Molecular and Optical Physics **41**, 105101 (2008).
[44] U. Fano, Physical Review **124**, 1866 (1961).
[45] Since RABITT experiments can not resolve s and d channels, the coupling between $3p \leftrightarrow ks$ and $3s \leftrightarrow kp$ also contributes, but only quantitatively.
[46] J. Wätzel, A. S. Moskalenko, Y. Pavlyukh, and J. Berakdar, Journal of Physics B: Atomic, Molecular and Optical Physics **48**, 025602 (2015).
[47] O. Gunnerson and B. Lundqvist, Physical Review B **13**, 4274 (1976).